

Seasonal increase of methane emissions linked to warming in Siberian tundra

Received: 19 April 2022

Accepted: 23 September 2022

Published online: 27 October 2022

 Check for updates

Norman Rößger^{1,2}, Torsten Sachs¹✉, Christian Wille¹, Julia Boike^{3,4} and Lars Kutzbach²✉

While increasing methane emissions from thawing permafrost are anticipated to be a major climate feedback, no observational evidence for such an increase has previously been documented in the literature. Here we report a trend of increasing methane emissions for the early summer months of June and July at a permafrost site in the Lena River Delta, on the basis of the longest set of eddy covariance methane flux data in the Arctic. Along with a strong air temperature rise of $0.3 \pm 0.1 \text{ °C yr}^{-1}$ in June, which corresponds to an earlier warming of 11 d, the methane emissions in June and July have increased by roughly $1.9 \pm 0.7\% \text{ yr}^{-1}$ since 2004. Although the tundra's maximum source strength in August has not yet changed, this increase in early summer methane emissions shows that atmospheric warming has begun to considerably affect the methane flux dynamics of permafrost-affected ecosystems in the Arctic.

Methane is an important greenhouse gas contributing roughly 16% to the radiative forcing from all well-mixed greenhouse gases¹. Current estimates² of the global methane source strength converge at 550–900 Tg yr⁻¹, with a contribution of $25 \pm 14 \text{ Tg yr}^{-1}$ from high-latitude wetlands in the Arctic tundra³. These wetlands and other inland waters form a globally relevant methane source and are the most important source of uncertainty in the global methane budget estimate². Reasons for this uncertainty include the shortage of flux observation sites and short time series, the high spatial heterogeneity of permafrost-affected landscapes, the pronounced temporal dynamics of methane emissions and the complex controls on methane production, transport and oxidation^{4–6}.

With a warming in the Arctic region that is at least twice the global average⁷, methane emissions are projected to increase in response to permafrost degradation⁸. This increase is anticipated to be driven by the remobilization of previously frozen soil organic matter or more specifically, by enhanced decomposition rates, an extension of the thawing season and a deepening of the seasonally thawed active layer into the perennially frozen layer underneath⁹. Increasing methane emissions are likely to lead to an additional rise in temperature, resulting in positive feedback with the potential to accelerate and further exacerbate climate change¹⁰. The resulting loss of permafrost is irreversible

at centennial time scales, particularly if permafrost thaw passes a tipping point¹¹. Currently, there is only moderate evidence with low agreement on whether northern permafrost regions are already releasing additional methane due to thaw⁸. Besides sparse indirect indications of increased carbon loss^{12,13}, neither atmospheric measurements nor inversion or biospheric models currently provide clear trends in methane emissions from high-latitude wetlands for the recent past¹⁴. It also remains unclear whether rising temperatures equally affect the two counteracting processes of methane production and oxidation⁶.

Here we analysed a methane flux dataset acquired over 16 yr between 2002 and 2019 in the North Siberian Lena River Delta (72° 22' 24.1' N, 126° 29' 49.7' E). This dataset currently forms the longest eddy covariance methane flux record from the Arctic, allowing for the first trend analysis of directly observed methane fluxes in an Arctic ecosystem. We also examined the dynamics in the fluxes, estimated annual and seasonal flux budgets, and identified flux drivers and proxies, which explain the observed fluxes on various time scales.

Flux trends and their seasonality

The trend analysis encompassed the 4 months June to September, with varying data availability throughout the years (Fig. 1).

¹GFZ German Research Centre for Geosciences, Telegrafenberg, Potsdam, Germany. ²Institute of Soil Science, Center for Earth System Research and Sustainability (CEN), Universität Hamburg, Hamburg, Germany. ³Alfred Wegener Institute for Polar and Marine Research, Telegrafenberg, Potsdam, Germany. ⁴Geography Department, Humboldt University of Berlin, Berlin, Germany. ✉e-mail: torsten.sachs@gfz-potsdam.de; lars.kutzbach@uni-hamburg.de

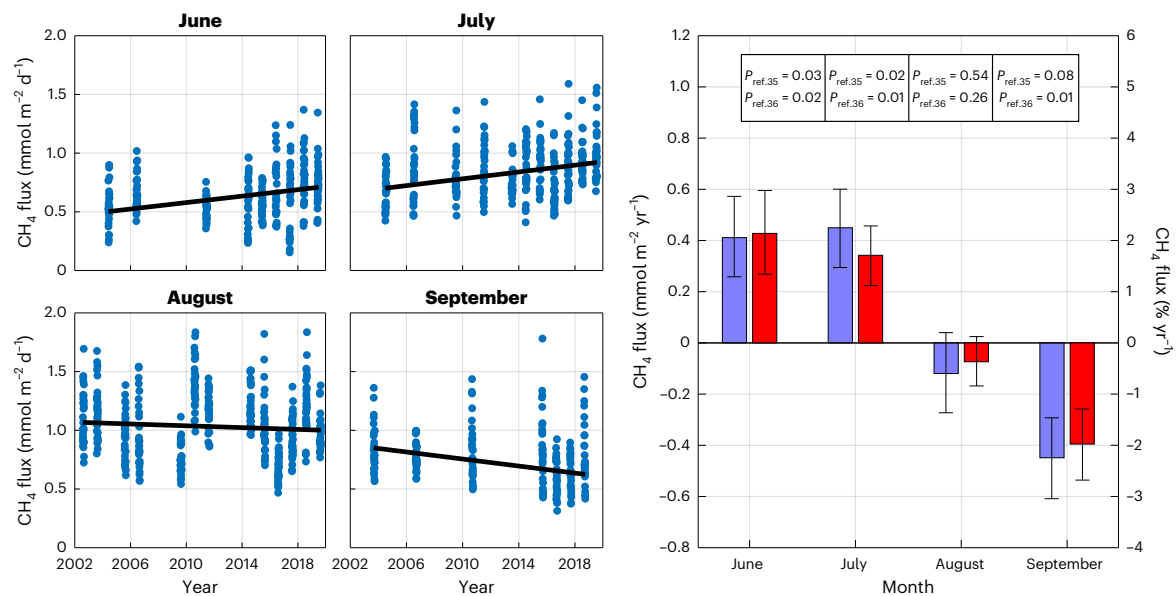


Fig. 1 | Methane flux trends during the 4-month thawing season. Left: gap-filled time series of daily means and their associated trend lines ($n_{June} = 270$, $n_{July} = 341$, $n_{August} = 403$, $n_{September} = 210$). Right: estimated absolute trends (left axis, blue bars) and estimated relative trends (right axis, red bars) for each month (same n as in left panel), including their uncertainties corresponding to the

95% confidence interval. P values were obtained from two modifications of the two-sided Mann-Kendall test after refs.^{35,36}. While the source strength increased in June and July, the peak emissions during August remained unchanged. These trends are consistent in sign and similar in significance when using non-gap-filled data only.

For June and July, we found statistically significant increases in methane emission of $0.41 \pm 0.16 \text{ mmol m}^{-2} \text{ yr}^{-1}$ ($2.1 \pm 0.8\% \text{ yr}^{-1}$) and $0.44 \pm 0.15 \text{ mmol m}^{-2} \text{ yr}^{-1}$ ($1.7 \pm 0.6\% \text{ yr}^{-1}$), respectively. The numbers in brackets denote the change relative to the monthly mean flux. These changes in early summer are equivalent to an increase of the mean annual methane budget by $0.5 \pm 0.1\%$ and are probably attributable to the significant air temperature rise of $0.3 \pm 0.1 \text{ }^\circ\text{C yr}^{-1}$ in June. This warming apparently had a larger effect on methanogenesis than on methanotrophy^{6,15} and corresponds to a significant increase in growing degree days (GDD) from $118 \text{ }^\circ\text{C}$ to $214 \text{ }^\circ\text{C}$ in June. Using $\text{GDD} = 60 \text{ }^\circ\text{C}$ as a benchmark for a representative cumulative heat input while maintaining high data coverage, the warming advanced towards the frozen season by $10.8 \pm 5.2 \text{ d}$ during the period from 2002 to 2019. Contrary to air temperature, we did not detect a significant soil temperature increase in the top soil layers (1 cm and 5 cm depth) and only a small and barely significant one at 10 cm depth in June. Similarly, there were no detectable trends in near-surface hydrology. We therefore assume the atmospheric warming to have caused an earlier onset of the vegetation period¹⁶, which in turn was probably a main driver of increased early summer methane emissions. The following mechanisms are considered to explain the relationship between air temperature (in addition to and independently of soil temperature changes) and methane emission in early summer. Higher air temperatures lead to both earlier snowmelt and onset of the development of the vegetation. Remote sensing also shows a greening in the Lena River Delta, with the strongest trends in the southern part along the main river channels where our site is located¹⁷. Graminoid vascular plants such as sedges which, together with mosses, dominate the local vegetation, have been described as benefitting most from earlier snowmelt and higher air temperature in spring¹⁸. Earlier development of vascular plants probably promotes earlier and stronger release of labile organic substances such as root exudates and fresh root litter into the rhizosphere¹⁹, providing substrates for the formation of methane^{20,21}. Its emission is promoted by the earlier foliating sedges that are known to foster upward methane transport through their extensive air spaces (aerenchyma), bypassing aerobic soil horizons and thus lowering the fraction of methane oxidized during

transport^{22,23}. An earlier development of vascular plants also promotes a decoupling of air and soil temperatures via both stronger radiation shading and higher evapotranspiration rates.

For August, we detected a marginal decline of $0.12 \pm 0.15 \text{ mmol m}^{-2} \text{ yr}^{-1}$ ($0.4 \pm 0.5\% \text{ yr}^{-1}$), with no statistically significant trend. Thus, the maximum source strength of the tundra has not changed. This stable state is supported by equally minor trends in the following two flux drivers: a rise in soil temperature (polygon centre, 30 cm depth) by $0.01 \pm 0.02 \text{ }^\circ\text{C yr}^{-1}$, which is similarly non-significant as the thaw depth that declined by $0.07 \pm 0.13 \text{ cm yr}^{-1}$. The thaw depth measurements, however, may be biased since they were conducted by mechanical probing, which can underestimate the degradation of permafrost due to a subsiding surface resulting from ground ice thaw and drainage.

For September, we found a decrease of $0.45 \pm 0.16 \text{ mmol m}^{-2} \text{ yr}^{-1}$ ($2.1 \pm 0.7\% \text{ yr}^{-1}$), which we did not consider a reliable trend since the two statistical tests disagreed on the significance. In addition, data availability was limited in September, leading air and soil temperature trends to change from positive to negative when their estimation was not based on all available temperature data, but only on data from those periods for which methane flux data were available. This change indicates that the selected 7 yr were not representative of the entire measurement period.

Flux budgets and dynamics

The methane fluxes were subject to an annual cycle for which we estimated a mean annual budget with a standard deviation of $171.5 \pm 12.3 \text{ mmol m}^{-2} \text{ yr}^{-1}$ (Fig. 2). This balance ranges between the lower quartile and the median of $236.9 \text{ mmol m}^{-2} \text{ yr}^{-1}$ in a right-skewed distribution, which was obtained from 168 annual budgets at various northern tundra sites²⁴. The reasons for the comparatively low fluxes at our site include the areal dominance of elevated polygon rims with non-water-saturated soils, the shallow active layer, the relatively low organic matter content²⁵ and one of the lowest mean ground temperatures in the northern hemisphere²⁶.

Roughly 61% of the mean annual budget can be ascribed to the thawing season, which begins in late May when air temperatures start

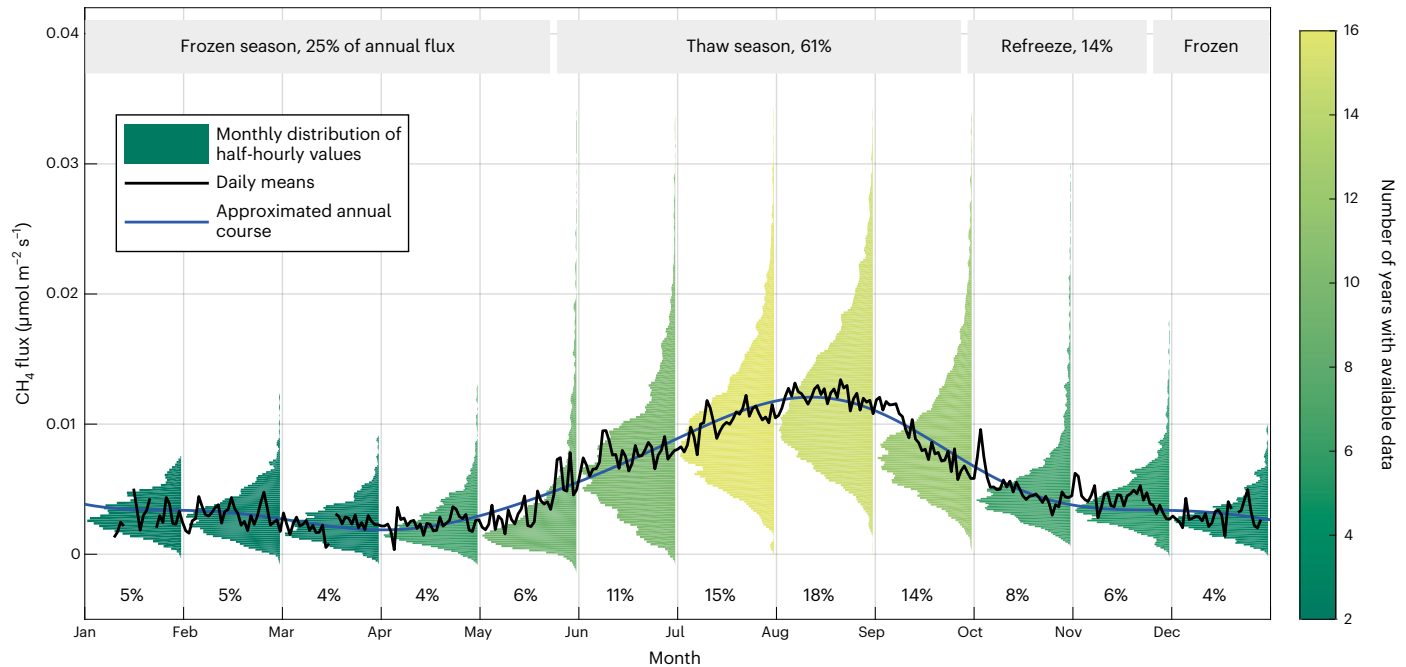


Fig. 2 | Mean annual cycle and data availability of methane fluxes as well as monthly and seasonal contributions to the budget. Monthly distributions of half-hourly methane fluxes and their mean annual course. The integration of the approximated course yielded a mean annual budget of $171.5 \pm 12.3 \text{ mmol m}^{-2} \text{ yr}^{-1}$. Mean monthly (percentages at the bottom) and seasonal (percentages at the top) contributions to the annual budget are indicated. The three seasons reflect the thermal state of the permafrost-affected soil. The thawing season began when

the surface temperature reached 0°C . When the surface temperature dropped below 0°C , the refreezing season was initiated. The frozen season began when sub-zero temperatures prevailed in the entire soil. While the emissions from the thawing season dominated the annual budget, the methane loss in the refreezing and frozen season was considerable given the cold conditions with little methanogenic activity.

to remain above freezing day and night and the snow has fully melted. In June, graminoid plant species begin to grow, thus facilitating upward methane transport through plant-mediated pathways²². The increasing fluxes reach their highest rates in early August, when the ground is thawed to a depth of approximately 50 cm. The rate of change in methane emissions during the subsequent drop in September is more pronounced than during the previous rise, leading to an asymmetric course around the flux peak. During the 4-month thawing season, the methane fluxes show a diurnal variation, with nocturnal fluxes being 7% lower on average than daytime fluxes (Fig. 3, top panels). Around early September, the vegetation period incrementally ceases, and in late September, a snow and ice cover develops, causing methane to start accumulating in a sub-surface stock between sporadic releases in the form of burst events (Fig. 4, top panels). With air temperatures already far below freezing, soil temperatures remain near 0°C during the zero-curtain period, allowing cold-adapted methanogenic archaea to remain active^{27,28} towards late November. This refreezing season accounts for about 14% of the mean annual budget. After the soil is completely frozen in December, methane fluxes continue to decrease at a slow pace by gradually depleting the soil methane pool, predominantly through diffusional processes. This frozen season, in which methanogenic microorganisms remain dormant, contributes around 25% to the mean annual budget.

Flux controls on various time scales

The methane fluxes and the explanatory power of associated flux drivers varied strongly on time scales from diurnal to inter-annual.

On the daily scale, the variations in methane fluxes were driven by friction velocity, which was also subject to a diurnal cycle (Fig. 3). This variable also influenced fluxes on the multi-day scale by driving methane bursts during stormy events that were associated with both friction velocity peaks and/or air pressure drops (Fig. 4). Friction velocity in particular affects soil–atmosphere coupling through pressure

pumping that enables advective trace gas transport rates through soil pores and the snowpack to increase far beyond molecular diffusion^{29,30}. This turbulence-induced process also facilitates methane transport across the air–water interface through bubble ebullition, that is, the intermittent release of undissolved methane trapped by adhesive forces, via agitation of plants and water³¹.

On the intra-annual scale, carbon dioxide fluxes determined with the eddy covariance method served as a proxy for methane fluxes between October and May (Fig. 5). During this refreezing and frozen season, the proportionality of methane and carbon dioxide fluxes (Fig. 5, top panel, left) suggests that their ratio in the pore space of soil and snow is rather invariant and that both trace gases were subject to the same physical transport processes. From June to August, thaw depth held explanatory power as an indicator of the maximum soil volume available for methanogenesis. However, this relationship was absent in September, when flux rates decreased despite near-maximum thaw depths. In September and October, surface albedo had a regulative influence, when it formed a proxy for enhancing snow coverage, and thus the decreasing coupling between ground and atmosphere. During the snowmelt in May, however, this coupling was less important due to both the ground being still largely frozen and its methane stock probably being depleted.

On the annual scale, a large part of the variability could be explained by air and soil temperatures as the fundamental variables driving metabolic processes such as methane production (Fig. 5). The soil temperature in a polygon centre at 20 cm depth was the best predictor compared with soil temperatures at other depths and locations within the polygon. This soil temperature reflects the water-saturated conditions in the centre, the timing of the annual thaw/freeze cycle and higher organic matter content in the top soil^{27,32}. The annual course of the air temperature preceded that of the methane flux, implicating hysteresis effects³³. Thus, the air temperature was most predictive, when described by two fits. The resulting apparent temperature sensitivities

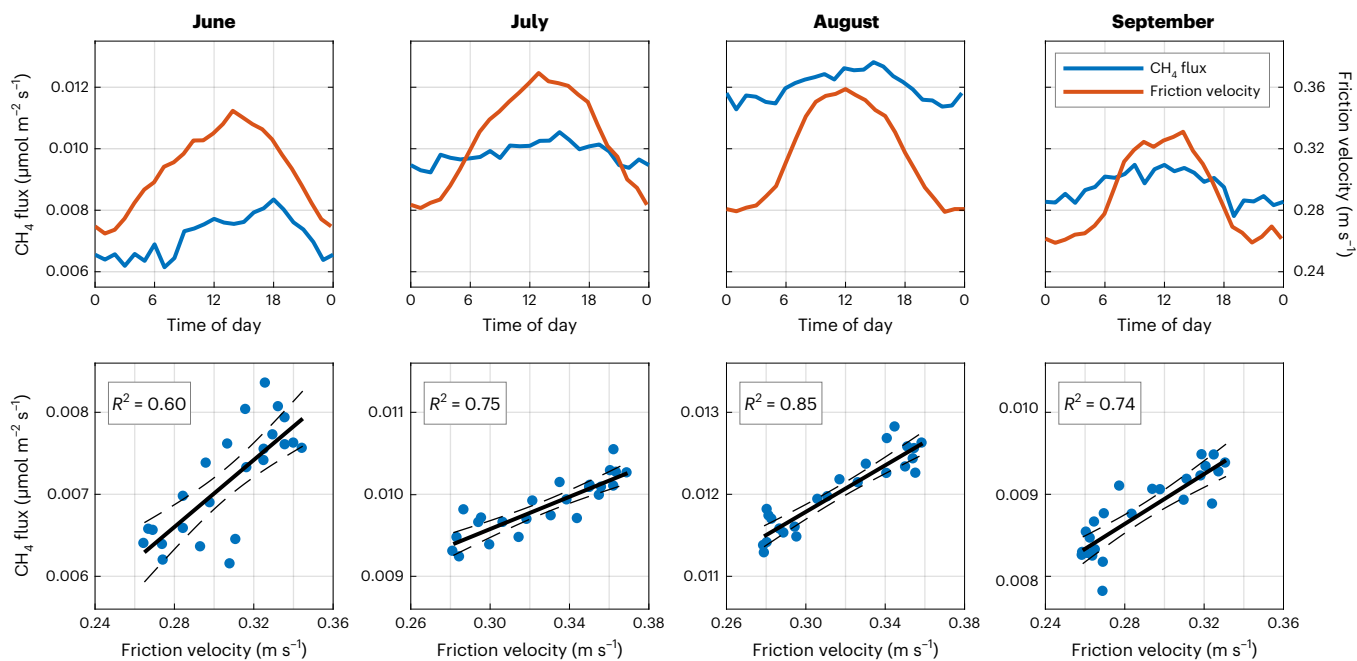


Fig. 3 | Variability and relationship between methane flux and friction velocity during the 4-month thawing season. Top: mean diurnal cycle of methane fluxes, with lower values at nighttime and elevated values at daytime induced by a similar evolution of friction velocity. Bottom: relationship between both variables on the diurnal scale illustrated with hourly means ($n = 24$ for each

month). The dashed lines around the solid regression functions denote the 95% confidence interval, while the goodness of fit is displayed by the coefficients of determination R^2 . Friction velocity impacts the surface–atmosphere coupling and hence affects methane transport rates, making it a reliable predictor of the daily flux variation.

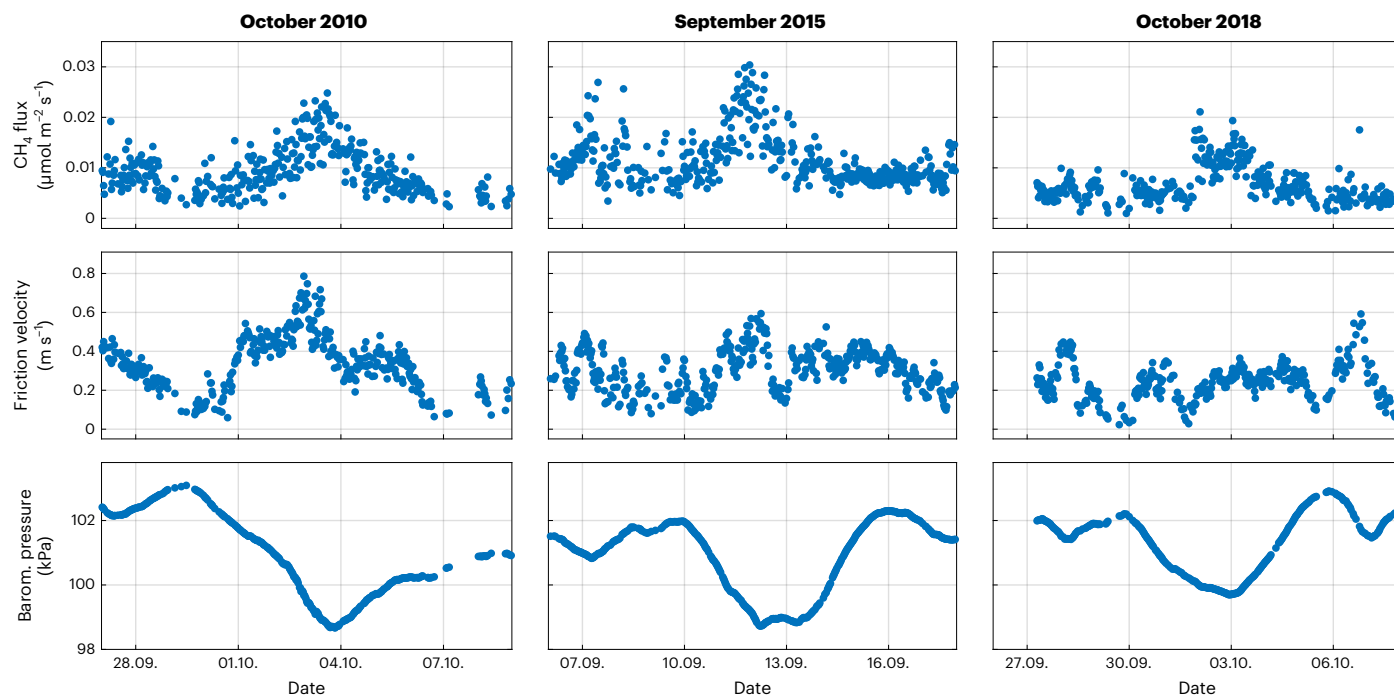


Fig. 4 | Implications of both friction velocity peaks and air pressure drops on methane efflux. Their effect was most pronounced during storms in September and October, when the sub-surface methane pool had been replenished in the preceding summer months.

(Q_{10}) were 1.9 (March to July) and 1.5 (August to February). This difference in Q_{10} values indicates that the methane fluxes appeared more responsive to changes in air temperatures during the early summer than thereafter, when soil temperatures were more influential. Besides air temperatures derived from observations, the annual variation was also well represented by air temperatures based on reanalysis

data³⁴. Their widespread availability thus offers the opportunity to estimate annual budgets or support regional flux upscaling in remote and sparsely inhabited tundra landscapes.

On the inter-annual scale, the period from 1 July to 15 September, which centres around the mean annual flux peak on 8 August, was taken into consideration for each year. Predictive power was provided by

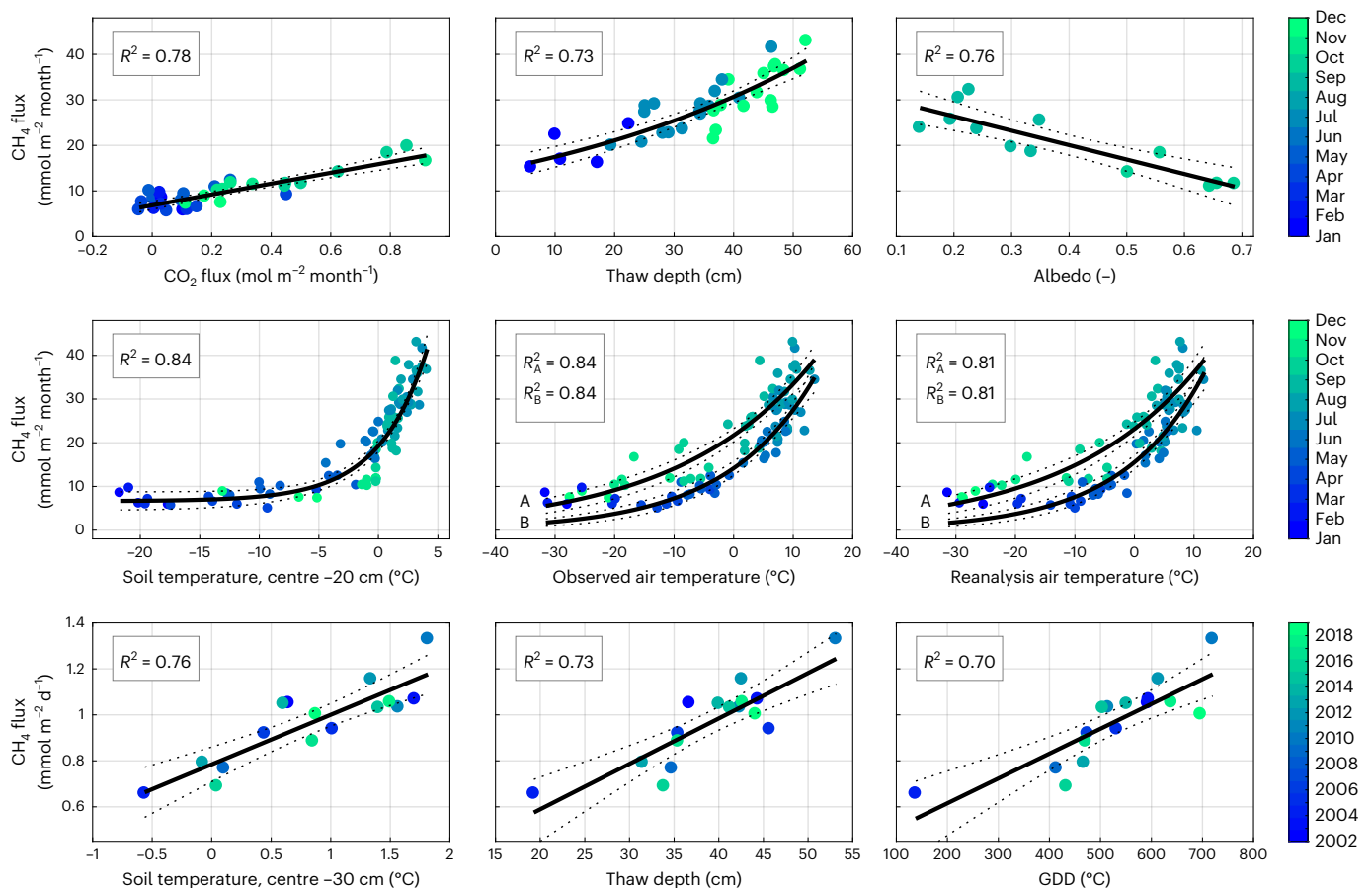


Fig. 5 | Relationships between methane flux and environmental variables at different time scales. The dotted lines around the solid regression functions designate the 95% confidence interval, while the goodness of fit is specified by the coefficients of determination. Top: intra-annual scale with monthly means of carbon dioxide flux (October to May, $n = 35$), thaw depth (June to August, $n = 41$) and surface albedo (September and October, $n = 18$). Middle: annual scale with monthly means of soil temperature ($n = 88$) as well as air temperature derived

from observational data ($n = 88$) and reanalysis data ($n = 88$). Curve A represents the period August to February, while curve B denotes the period March to July. Bottom: inter-annual scale, covering the period 1 July to 15 September, with means of soil temperature ($n = 16$), thaw depth ($n = 16$) and growing degree days ($n = 16$). The explanatory power of each environmental variable varied along both time scale and analysis period due to the complex temporal variability of the methane fluxes.

variables that best describe this maximum development stage of the ecosystem: soil temperature in a polygon centre at 30 cm depth, thaw depth and growing degree days (Fig. 5). The explanatory power of growing degree days was not diminished when observed air temperatures were replaced with air temperatures from reanalysis data³⁴.

Conclusion

Earth system models project an increased carbon release from permafrost-affected landscapes due to climate change, albeit there has been little agreement on timing and magnitude due to observational constraints and an incomplete knowledge on drivers and relationships¹⁴. To our knowledge, we provide the first observational evidence of an increasing trend of early summer methane emissions from tundra wetlands linked to atmospheric warming. The observed trends may still be moderate, yet they constitute a notable development given the very thick and cold continuous permafrost in the study area compared with most other observational sites. We also provide further support for the importance of the cold season, in which we estimate 39% of the total annual methane to be released while continuous data coverage remains a substantial challenge in the Arctic winter.

Online content

Any methods, additional references, Nature Research reporting summaries, source data, extended data, supplementary information,

acknowledgements, peer review information; details of author contributions and competing interests; and statements of data and code availability are available at <https://doi.org/10.1038/s41558-022-01512-4>.

References

- Butler, J. H. & Montzka, S. A. *The NOAA Annual Greenhouse Gas Index* (NOAA, 2021).
- Saunio, M. et al. The global methane budget 2000–2017. *Earth Syst. Sci. Data* **12**, 1561–1623 (2020).
- Parmentier, F.-J. W. et al. A synthesis of the Arctic terrestrial and marine carbon cycles under pressure from a dwindling cryosphere. *Ambio* **46**, 53–69 (2017).
- McGuire, A. D. et al. Sensitivity of the carbon cycle in the Arctic to climate change. *Ecol. Monogr.* **79**, 523–555 (2009).
- McGuire, A. D. et al. An assessment of the carbon balance of Arctic tundra: comparisons among observations, process models, and atmospheric inversions. *Biogeosciences* **9**, 3185–3204 (2012).
- Oh, Y. et al. Reduced net methane emissions due to microbial methane oxidation in a warmer Arctic. *Nat. Clim. Change* **10**, 317–321 (2020).
- Masson-Delmotte, V. et al. in *Climate Change 2013: The Physical Science Basis* (eds Stocker, T. F. et al.) Ch. 5 (IPCC, Cambridge Univ. Press, 2013).

8. Meredith, M. et al. in *IPCC Special Report on the Ocean and Cryosphere in a Changing Climate* (eds Pörtner, H.-O. et al.) Ch. 3 (IPCC, Cambridge Univ. Press, 2019).
9. Schuur, E. A. G. et al. Vulnerability of permafrost carbon to climate change: implications for the global carbon cycle. *Bioscience* **58**, 701–714 (2008).
10. Dean, J. F. et al. Methane feedbacks to the global climate system in a warmer world. *Rev. Geophys.* **56**, 207–250 (2018).
11. Lenton, T. M. et al. Climate tipping points — too risky to bet against. *Nature* **575**, 592–595 (2019).
12. Wild, B. et al. Rivers across the Siberian Arctic unearth the patterns of carbon release from thawing permafrost. *Proc. Natl Acad. Sci. USA* **116**, 10280–10285 (2019).
13. Walter Anthony, K. et al. Methane emissions proportional to permafrost carbon thawed in Arctic lakes since the 1950s. *Nat. Geosci.* **9**, 679–682 (2016).
14. Canadell, J. G. et al. in *Climate Change 2021: The Physical Science Basis* (eds Masson-Delmotte, V. et al.) Ch. 5 (IPCC, Cambridge Univ. Press, 2021).
15. Dunfield, P., Knowles, R., Dumont, R. & Moore, T. R. Methane production and consumption in temperate and subarctic peat soils: response to temperature and pH. *Soil Biol. Biochem.* **25**, 321–326 (1993).
16. Kelsey, K. C. et al. Winter snow and spring temperature have differential effects on vegetation phenology and productivity across Arctic plant communities. *Glob. Change Biol.* **27**, 1572–1586 (2021).
17. Nitze, I. & Grosse, G. Detection of landscape dynamics in the Arctic Lena Delta with temporally dense Landsat time-series stacks. *Remote Sens. Environ.* **181**, 27–41 (2016).
18. Livensperger, C. et al. Earlier snowmelt and warming lead to earlier but not necessarily more plant growth. *AoB Plants* **8**, plw021 (2016).
19. Chanton, J. P. et al. Radiocarbon evidence for the importance of surface vegetation on fermentation and methanogenesis in contrasting types of boreal peatlands. *Global Biogeochem. Cycles* **22**, GB4022 (2008).
20. Joabsson, A. & Christensen, T. R. Methane emissions from wetlands and their relationship with vascular plants: an Arctic example. *Glob. Change Biol.* **7**, 919–932 (2001).
21. Bridgman, S. D., Cadillo-Quiroz, H., Keller, J. K. & Zhuang, Q. Methane emissions from wetlands: biogeochemical, microbial, and modeling perspectives from local to global scales. *Glob. Change Biol.* **19**, 1325–1346 (2013).
22. Kutzbach, L., Wagner, D. & Pfeiffer, E. M. Effect of microrelief and vegetation on methane emission from wet polygonal tundra, Lena Delta, Northern Siberia. *Biogeochemistry* **69**, 341–362 (2004).
23. Dorodnikov, M., Knorr, K. H., Kuzyakov, Y. & Wilmking, M. Plant-mediated CH₄ transport and contribution of photosynthates to methanogenesis at a boreal mire: a ¹⁴C pulse-labeling study. *Biogeosciences* **8**, 2365–2375 (2011).
24. Treat, C. C., Bloom, A. A. & Marushchak, M. E. Nongrowing season methane emissions – a significant component of annual emissions across northern ecosystems. *Glob. Change Biol.* **24**, 3331–3343 (2018).
25. Knoblauch, C., Spott, O., Evgrafova, S., Kutzbach, L. & Pfeiffer, E. M. Regulation of methane production, oxidation, and emission by vascular plants and bryophytes in ponds of the northeast Siberian polygonal tundra. *J. Geophys. Res. Biogeosci.* **120**, 2525–2541 (2015).
26. Obu, J. et al. Northern Hemisphere permafrost map based on TTOP modelling for 2000–2016 at 1km² scale. *Earth Sc. Rev.* **193**, 299–316 (2019).
27. Wagner, D. et al. Methanogenic activity and biomass in Holocene permafrost deposits of the Lena Delta, Siberian Arctic and its implication for the global methane budget. *Glob. Change Biol.* **13**, 1089–1099 (2007).
28. Rivkina, E. et al. Microbial life in permafrost. *Adv. Space Res.* **33**, 1215–1221 (2004).
29. Bowling, D. R. & Massman, W. J. Persistent wind-induced enhancement of diffusive CO₂ transport in a mountain forest snowpack. *J. Geophys. Res. Biogeosci.* **116**, G04006 (2011).
30. Takle, E. S. et al. Influence of high-frequency ambient pressure pumping on carbon dioxide efflux from soil. *Agric. Meteorol.* **124**, 193–206 (2004).
31. Wille, C., Kutzbach, L., Sachs, T., Wagner, D. & Pfeiffer, E.-M. Methane emission from Siberian Arctic polygonal tundra: eddy covariance measurements and modeling. *Glob. Change Biol.* **14**, 1395–1408 (2008).
32. Walz, J., Knoblauch, C., Böhme, L. & Pfeiffer, E. M. Regulation of soil organic matter decomposition in permafrost-affected Siberian tundra soils - impact of oxygen availability, freezing and thawing, temperature, and labile organic matter. *Soil Biol. Biochem.* **110**, 34–43 (2017).
33. Chang, K. Y. et al. Substantial hysteresis in emergent temperature sensitivity of global wetland CH₄ emissions. *Nat. Commun.* **12**, 2266 (2021).
34. *The NCEP/NCAR Reanalysis Project* (NOAA, 2019); <https://psl.noaa.gov/data/reanalysis>
35. Hamed, K. & Rao, R. A modified Mann-Kendall trend test for autocorrelated data. *J. Hydrol.* **204**, 182–196 (1998).
36. Yue, S. & Wang, C. The Mann-Kendall test modified by effective sample size to detect trend in serially correlated hydrological series. *Water Resour. Manage.* **18**, 201–218 (2004).

Publisher's note Springer Nature remains neutral with regard to jurisdictional claims in published maps and institutional affiliations.

Open Access This article is licensed under a Creative Commons Attribution 4.0 International License, which permits use, sharing, adaptation, distribution and reproduction in any medium or format, as long as you give appropriate credit to the original author(s) and the source, provide a link to the Creative Commons license, and indicate if changes were made. The images or other third party material in this article are included in the article's Creative Commons license, unless indicated otherwise in a credit line to the material. If material is not included in the article's Creative Commons license and your intended use is not permitted by statutory regulation or exceeds the permitted use, you will need to obtain permission directly from the copyright holder. To view a copy of this license, visit <http://creativecommons.org/licenses/by/4.0/>.

© The Author(s) 2022

Methods

Site description

The Lena River Delta is located within the zone of continuous permafrost on the fringe of the Laptev Sea in northern Siberia. The delta region is situated in a continental Arctic climate with a mean annual air temperature of $-12.3\text{ }^{\circ}\text{C}$ and a mean annual precipitation of 169 mm (ref. ³⁷). One of the numerous islands is Samoylov Island, which has been hosting researchers from various fields since the late 1980s. The flux tower was established on the late Holocene river terrace, whose patterned ground has been shaped by frost action processes that created an ice-wedge polygonal tundra with thermokarst lakes and ponds. This landscape is characterized by a mosaic of depressed polygon centres, which often have a moist to wet water regime supporting hydrophytic sedges and mosses, as well as elevated polygon rims, which remain moist to moderately dry and covered by mesophytic sub-shrubs, mosses and lichen²².

Instrumental setup

An eddy covariance system was set up in July 2002 to determine turbulent fluxes of energy and matter. During the period 2002–2006, the measurement system consisted of a Gill Instruments R3 sonic anemometer, a LI-COR Li-7000 $\text{CO}_2/\text{H}_2\text{O}$ gas analyser and a Campbell Scientific TGA-100 closed-path CH_4 gas analyser. After a break in 2007 and 2008, methane flux observations restarted in 2009 with a system consisting of a Campbell Scientific CSAT3 sonic anemometer, a LI-COR Li-7500 $\text{CO}_2/\text{H}_2\text{O}$ gas analyser and a Los Gatos Research FMA Model 907-0001 closed-path CH_4 gas analyser. In 2010, we added a LI-COR Li-7000 $\text{CO}_2/\text{H}_2\text{O}$ gas analyser and a LI-COR Li-7700 open-path CH_4 gas analyser to the setup. Initially, the observations were conducted on the basis of field campaigns that lasted 2–4 months. After the commissioning of a new, permanently staffed research station in 2013, we upgraded the measurement system successively to enable year-round operation. Within the scope of these measures, a new flux tower was erected very close to the previous tower, and a Los Gatos FGA-24r-EP Model 911-0010-0002 closed-path $\text{CH}_4/\text{CO}_2/\text{H}_2\text{O}$ gas analyser was put into operation in an air-conditioned field lab in 2018. From the outset, flux observations were complemented by meteorological, hydrological and soil physical measurements³⁷ at the flux tower as well as other sites on Samoylov Island. Records until September 2019 were analysed in this study.

Flux processing

Half-hourly fluxes were calculated with the EddyPro³⁸ software (version 6.2.2). As part of the initial raw data processing, we implemented a double rotation tilt correction to reduce the means of both lateral and vertical wind to zero. Turbulent fluctuations of the wind and gas concentration signals were extracted by trend removal through an exponential running mean, with a time constant of 30 s during 2002 to 2009 and a linear detrending from 2010 onwards. Time lags between wind and gas concentration signals were identified by covariance maximization and compensated for by applying setup-specific plausible time lag windows and defaults. After the actual flux calculation, we subsequently corrected these fluxes using the WPL correction³⁹ to account for fluctuations in heat and water vapour in the air. We then conducted a correction to account for high-pass filtering⁴⁰ due to a finite averaging interval, and low-pass filtering⁴¹ due to both sensor separation and sensor imperfection. When methane fluxes from both open-path and closed-path gas analysers were available, only the fluxes determined from closed-path gas concentration data were used for further processing.

The calculated methane fluxes underwent a comprehensive quality assessment routine with various individual steps to ensure that only reliable fluxes were interpreted. We initiated this procedure with the raw data screening, where half-hourly time intervals were discarded when the measured methane concentrations did not lie between the limits 1 and 3 ppm and/or the number of spikes⁴² for the three wind vectors and the methane concentration exceeded 5. Subsequently, we

identified fluxes with non-steady-state conditions using a stationarity test⁴³. These fluxes were removed, as well as the fluxes that did not pass the integral turbulence characteristics test⁴³ due to an absence of turbulent conditions. To further recognize a deficiently developed turbulence as well as instrument malfunctions, we examined the skewness and kurtosis⁴⁴ of flux-specific scalars. Fluxes were dismissed when the skewness was either less than -2 or greater than 2 and/or kurtosis was less than 1 or greater than 8 . In addition to these steps, we filtered the open-path fluxes according to the following steps. To ensure that the WPL correction³⁹ was not distorted by poor-quality data, we rejected methane fluxes if the corresponding sensible and latent heat fluxes had failed the preceding quality assurance. Further steps involved discarding fluxes when the signal strength (that is, the available optical power in the laser path of the methane analyser) was below 10%. Fluxes were also removed when lags determined by the time lag compensation was outside the interval of -2 to $+2$ s. Finally, we computed the percentiles for the leftover methane fluxes, and fluxes below the 1st percentile and above the 99th percentile were excluded.

The remaining data formed the basis for further analysis and included 70,202 half-hourly methane flux records that were observed during 1,986 d within 16 yr. The thawing, refreezing and frozen seasons account for 63%, 13% and 24% of these records, respectively. To our knowledge, this is the most comprehensive eddy covariance methane flux dataset available from an Arctic permafrost-affected ecosystem.

Flux budget estimation

At first, we computed a mean flux and its standard deviation for each calendar day using half-hourly fluxes. These daily means formed a mean annual course that was then approximated with a Fourier series whose integration yielded the mean annual budget. Its uncertainty was obtained by processing the standard deviations with standard error propagation techniques. We used three standard deviations around the mean ($\mu \pm 3\sigma$) and the few missing standard deviations for some winter days were replaced with monthly means. The cumulative flux, F_{CH_4} , was calculated as

$$F_{\text{CH}_4} = \int_{0.5}^{365.5} a_0 + \sum_{i=1}^3 a_i \times \cos(i \times x \times w) + b_i \times \sin(i \times x \times w) dx,$$

where i is the index of summation, x depicts the annual time scale as calendar days, and a , b and w symbolize fitting parameters derived through least squares regression. The mean annual course could be well reproduced as shown by a coefficient of determination of 0.93.

The mean annual budget was allocated to three seasons, which we defined on the basis of the soil's thermal state. The thawing season began on 24 May when the daily mean surface temperature (determined via the outgoing long-wave radiation) exceeded the freezing point. When the surface temperature again dropped below zero around 27 September, the following refreezing season started. The subsequent 'frozen' season began when sub-zero temperatures prevailed in the entire soil from 23 November onwards.

Flux driver search

In search of adequate predictors on different time scales, the relationship between observed fluxes and potential flux drivers was analysed by means of simple least squares regression. In doing so, we isolated the respective effect of individual flux drivers (while neglecting the mutual effect of multiple flux drivers) to compare their explanatory power. In many cases, a linear fit was applied. The uncertainty in the functional relationships was assessed with 95% confidence intervals. For characterizing the relationship with soil temperatures on the annual scale, we used an exponential approach, whose curve flattening well depicted the low but steady emissions during the frozen season.

$$F_{\text{CH}_4} = b_1 \times e^{b_2 \times T_{\text{soil}}} + b_3$$

F_{CH_4} denotes the methane flux, T_{soil} represents the soil temperature and b_{1-3} refer to the coefficients to be estimated. For the curve fitting of fluxes with thaw depth as a predictor, we used the same parameterization but excluding the coefficient ' b_3 '. The effect of air temperature on methane emissions was well described by classic Q_{10} relationships⁴⁵, which provided additional information on the temperature sensitivity of the emissions.

$$F_{\text{CH}_4} = F_{\text{base}} \times Q_{10}^{\frac{T_{\text{air}} - T_{\text{ref}}}{10}}$$

F_{base} describes the basal emission at the reference temperature T_{ref} which was set to 15 °C, and the scaling factor⁴⁶ γ was held constant at 10 °C. Q_{10} indicates the temperature sensitivity and specifies a value by which the emission multiplies/divides when the temperature rises/drops by 10 °C. These two fitting parameters, however, disregard the effect of various other hydrometeorological and biogeochemical factors on methane fluxes, and thus rather state an apparent temperature response. The correlation between flux and environmental variables was assessed with the coefficient of determination.

For the determination of growing degree days, we averaged the daily maximum and minimum air temperatures for each day. This mean was adopted if it was greater than the base temperature of 0 °C; otherwise, it was set to zero. Subsequently, we determined the cumulative sum of all daily values for each year. Using data for growing degree days, soil temperatures and thaw depths in investigating the year-to-year variability depended on the availability of methane fluxes: for each year, we calculated a mean flux that was based on data between 1 July and 15 September. The means of the three predictors were then computed using only data from time intervals when fluxes were available.

Flux modelling

For filling the gaps in the methane flux time series, we implemented a random forest^{47,48}, that is, a supervised algorithm which is robust with respect to noise and is able to deal with nonlinear relationships, complex interactions as well as missing data. Its error rates compare favourably with other machine learning techniques. The forest consists of a large collection of individual regression trees that operate as an ensemble. Each tree is based on a bootstrapped dataset of observational features, with duplicate samples being allowed. Growing the roots and splits of each tree occurs through a random subset of features in each bootstrapped dataset. Therefore, each leaf corresponds to the average flux rate from a distinctly different cluster of observations. The randomly varying data input (in terms of both samples and features) in the course of the growing process results in a wide variety of de-correlated trees, which constitutes a favourable way to resolve the bias-variance trade-off in the random forest. Its performance was further enhanced by manually tuning inherent hyperparameters (minimum leaf size, maximum number of splits, number of learning cycles), while its complexity for optimal predictive power was assessed through 10-fold cross validation.

On the basis of the outcome of the previous regression analysis, we constrained the model with daily means of (1) air temperatures and soil temperatures from a polygon centre in 20 cm depth to reflect methane production, (2) air pressure and friction velocity to account for methane transport and (3) surface albedo and thaw depth to provide additional explanatory power during the shoulder seasons and the summer flux peak period when the temporal variability was greater than in the winter. To avoid multicollinearity among the six predictor variables, we carried out two tests⁴⁹. The largest condition index and variance inflation factor were 7.9 and 3.3, respectively, and thus well below 30 and 10, above which these scores are indicative of problematic multicollinearity. The model was able to reproduce the observed fluxes well and yielded, in the absence of heteroscedasticity, a coefficient of determination of 0.75. The mean absolute error was 138.2 $\mu\text{mol m}^{-2} \text{d}^{-1}$, which translates to a mean relative error of 18.7%.

Flux trend evaluation

To detect changes in emission rates of individual months over several years, we only used months with a minimum fraction of 30% of observed fluxes and full data coverage after gap-filling. Importantly, using non-gap-filled data for trend analyses resulted in trends consistent in sign and similar in significance. Thus, using gap-filled data compensates for uneven data distribution across the years and allows for robust trend estimation without introducing artefacts. Following these criteria resulted in June, July, August and September being eligible for analysis, for which data from 9, 11, 13 and 7 yr were respectively available.

We assessed upward or downward changes in methane fluxes over time by fitting a trend line following the Theil-Sen approach. The major advantage of this method is its insensitivity to outliers, whose impact would naturally be larger in our 16 yr dataset compared with the 30 yr period that is traditionally used for the characterization of climates. The magnitude of the trend corresponded to the slope of the obtained trend line. We further divided this absolute trend by the monthly flux mean to obtain the relative trend. The associated uncertainty was given using the 95% confidence interval of the trend line. The trend estimation for other environmental variables was conducted in an equivalent manner.

The statistical significance of the trend was examined using two modifications of the two-sided Mann-Kendall test^{35,36} that both take into account the effect of serial correlation in time series on the probability of trend detection. The objective of using two tests was to find a trade-off between the power of both tests and their capability to preserve the commonly adopted significance level of 0.05 against the background of limited data availability⁵⁰. Within the given uncertainty range, we considered a trend present or absent when both tests led to the same outcome, whereas opposed test statistics indicate minor confidence in the decision on trend detection.

Data availability

The dataset analysed in this study is available from the corresponding author upon request and at the European Fluxes Database Cluster under site ID RU-Sam.

Code availability

The code to reproduce the results of this study is available from GFZ Data Services: <https://doi.org/10.5880/GFZ.1.4.2022.010> (ref. ⁵¹).

References

- Boike, J. et al. A 16-year record (2002–2017) of permafrost, active-layer, and meteorological conditions at the Samoylov Island Arctic permafrost research site, Lena River delta, northern Siberia: an opportunity to validate remote-sensing data and land surface, snow, and permafrost models. *Earth Syst. Sci. Data* **11**, 261–299 (2019).
- Eddy Covariance Processing Software (LI-COR Biosciences, 2017).
- Webb, E. K., Pearman, G. I. & Leuning, R. Correction of flux measurements for density effects due to heat and water vapour transfer. *Q. J. R. Meteorol. Soc.* **106**, 85–100 (1980).
- Moncrieff, J. B., Clement, R., Finnigan, J. & Meyers, T. in *Handbook of Micrometeorology. A Guide for Surface Flux Measurement and Analysis* (eds Lee, X. et al.) 7–31 (Springer, 2004).
- Fratini, G., Ibrom, A., Arriga, N., Burba, G. & Papale, D. Relative humidity effects on water vapour fluxes measured with closed-path eddy-covariance systems with short sampling lines. *Agric. Meteorol.* **165**, 53–63 (2012).
- Vickers, D. & Mahrt, L. Quality control and flux sampling problems for tower and aircraft data. *J. Atmos. Ocean. Technol.* **14**, 512–526 (1997).
- Foken, T. & Wichura, B. Tools for quality assessment of surface-based flux measurements. *Agric. Meteorol.* **78**, 83–105 (1996).

44. Tennekes, H. & Lumley, J. L. *A First Course in Turbulence* (MIT Press, 1972).
45. van't Hoff, J. H. in *Lectures on Theoretical and Physical Chemistry: Part I: Chemical Dynamics* 224–229 (Edward Arnold, 1898).
46. Mahecha, M. D. et al. Global convergence in the temperature sensitivity of respiration at ecosystem level. *Science* **329**, 838–840 (2010).
47. Breiman, L. Random forests. *Mach. Learn.* **45**, 5–32 (2001).
48. Hastie, T., Tibshirani, R. & Friedman, J. *The Elements of Statistical Learning. Data Mining, Inference, and Prediction* Springer Series in Statistics (Springer, 2009). <https://doi.org/10.1007/978-0-387-84858-7>
49. Belsley, D. A., Kuh, E. & Welsh, R. E. *Regression Diagnostics: Identifying Influential Data and Sources of Collinearity* (John Wiley & Sons, 1980).
50. Blain, G. C. The modified Mann-Kendall test: on the performance of three variance correction approaches. *Bragantia* **72**, 416–425 (2013).
51. Rößger, N., Sachs, T., Wille, C., Boike, J. & Kutzbach, L. Methane flux trend analysis, *GFZ Data Services*, 1.0, <https://doi.org/10.5880/GFZ.1.4.2022.010> (2022).

Acknowledgements

Financial support was provided by the German Ministry of Education and Research (CarboPerm Project, BMBF grant number 03G0836A, L.K.; KoPf Project, BMBF grant number 03F0764A, L.K.), the European Union Seventh Framework Programme (PAGE21 project, EU contract number GA282700, L.K., J.B.), the European Union's Horizon 2020 research and innovation programme (grant number 689443, T.S.) via project iCUPE, the Helmholtz Association of German Research Centres (grant VH-NG-821, T.S. and ACROSS project, J.B.) and the Cluster of Excellence CliSAP at the University of Hamburg (EXC177, DFG project number 38787541, L.K.). This article is a contribution to the Cluster of Excellence 'CLICCS - Climate, Climatic Change, and Society' (EXC 2037, DFG project number 390683824, L.K.) funded by the German

Research Foundation, and a contribution to the Center for Earth System Research and Sustainability at University of Hamburg. We thank the Arctic and Antarctic Research Institute, St. Petersburg, the Melnikov Permafrost Institute, Yakutsk, the Trofimuk Institute of Petroleum Geology and Geophysics, Novosibirsk, the Lena Delta Reserve, Tiksi, the staff of the research station on Samoylov Island as well as the numerous Russian and German colleagues involved in expedition organization, logistics and technical field support throughout the many years. We especially thank E.-M. Pfeiffer for initiating the eddy covariance greenhouse gas monitoring in the Lena River Delta.

Author contributions

N.R., L.K., C.W. and T.S. designed the study. N.R., T.S., C.W., J.B. and L.K. acquired the data through field work. N.R. and C.W. conducted the raw data processing. N.R. analysed the data. N.R., T.S., C.W. and L.K. interpreted and iterated analyses. N.R. wrote the article with contributions from C.W. and revisions by T.S., C.W., J.B. and L.K.

Funding

Open access funding provided by Helmholtz-Zentrum Potsdam Deutsches GeoForschungsZentrum - GFZ.

Competing interests

The authors declare no competing interests.

Additional information

Correspondence and requests for materials should be addressed to Torsten Sachs or Lars Kutzbach.

Peer review information *Nature Climate Change* thanks Elodie Salmon, Timo Vesala and the other, anonymous, reviewer(s) for their contribution to the peer review of this work.

Reprints and permissions information is available at www.nature.com/reprints.